International Journal of Heat and Mass Transfer 52 (2009) 2311–2323

Contents lists available at ScienceDirect

International Journal of Heat and Mass Transfer

journal homepage: www.elsevier.com/locate/ijhmt

Experimental study on condensation heat transfer inside a single circular minichannel

Marko Matkovic *, Alberto Cavallini, Davide Del Col, Luisa Rossetto

Dipartimento di Fisica Tecnica, Università degli Studi di Padova, Via Venezia 1, 35131 Padova, Italy

ARTICLE INFO

Article history:
Received 14 February 2008
Available online 12 January 2009

Keywords:
Condensation
Minichannels
Local heat transfer coefficient
Refrigerants
Experimentation

ABSTRACT

The measurement of the condensation heat transfer coefficient inside micro- and minichannels is still somewhat elusive due to the difficult task of getting accurate values of the heat transfer coefficients during the condensation process, particularly when studied within single minichannels. The present paper reports local heat transfer coefficients obtained from the measurement of the local heat flux and the direct measurement of the saturation and wall temperatures during condensation of R134a and R32 within a single circular 0.96 mm diameter minichannel. Except for the lowest mass velocity, the test results do not show significant discrepancy from the trends expected for macroscale tubes.

1. Introduction

Micro- and minichannels are increasingly being used to achieve high heat transfer rates with compact heat exchangers. Condensation inside small diameter channels finds applications in heat pipes and compact heat exchangers for electronic equipment or spacecraft thermal control, in automotive condensers, in residential air conditioning and in refrigeration applications.

In addition to high heat flux applications, micro- and minichannels are viewed as appropriate options for reducing inventories of hazardous fluids and also reducing greenhouse gas emissions by improving component and system energy efficiency. The compactness of minichannel elements in air-cooled condensers improves the system efficiency through out the reduction of air-side pressure drops and the increase of the heat transfer coefficients. The adoption of minichannels also promotes the reduction of the refrigerant charge, which is favourable to the use of toxic or flammable refrigerants. Furthermore, small diameter channels can be well used with high pressure fluids, for instance with carbon dioxide in transcritical cycle equipment, since these elements are able to withstand high system pressures.

It should be noted that such compact condensers have been designed and used for some years by the automotive industry, where air-conditioning condensers consist of rectangular tubes with multiple parallel minichannels cooled by air flowing across fins. The minichannels used in these condensers often have hydraulic diameters in the 0.5–1.5 mm range.

Researchers have discussed the terms "microchannel" and "minichannel" at some length in the literature. As suggested by some authors, microchannel phase change may differ from the similar process in conventional channels due to differences in the relative influence of gravity, shear stress and surface tension. Whereas some transition criteria between macro- and microscale channels have been proposed with reference to the flow boiling process, no specific criteria have been developed for the definition of mini- and/or microchannels during forced convective condensation. In the present paper, the classification taken from Kandlikar and Grande [1] is adopted and therefore minichannels can be single tubes or multiport extruded aluminum channels having inner hydraulic diameters d_h in the range 0.2–3 mm.

While two-phase flow, evaporation, and boiling in mini- and microchannels have received considerable attention in the recent past, due to the growing interest in the high heat fluxes made possible by this geometry, condensation in such channels has been studied by fewer investigators.

The measurement of condensation heat transfer coefficients, however, is somewhat elusive and the number of available experimental data relative to condensation inside minichannels is rather limited. One of the reasons is that unlike in the case of evaporation and boiling, where heat transfer rates can be accurately measured based on the direct determination of electrical heat input, condensation heat transfer rates have to be determined indirectly. The small flow rates in minichannels result in small heat transfer rates, particularly if the measurements are to be conducted across small quality increments in the vapour–liquid dome. Furthermore, the

* Corresponding author. Tel.: +39 049 827 6891; fax: +39 049 827 6896.
E-mail addresses: marko.matkovic@guest.arnes.si (M. Matkovic), davide.delcol@unipd.it (D. Del Col).

0017-9310/$ - see front matter © 2008 Elsevier Ltd. All rights reserved.
doi:10.1016/j.ijheatmasstransfer.2008.11.013

Nomenclature

c_p	specific heat capacity [J kg^{-1} K^{-1}]
d	diameter [m]
G	mass velocity [kg m^{-2} s^{-1}]
h_{LG}	latent heat [J kg^{-1}]
L	total length of the measuring sector [m]
q'	heat flux (referred to the inner surface) [W m^{-2}]
q	heat flow rate [W]
T	temperature [K, °C]
x	thermodynamic vapour quality [/]
z	axial position [m]
α, HTC	heat transfer coefficient [W m^{-2} K^{-1}]
δ	absolute error associated to the measured/calculated value
ΔT	temperature difference [K]

Other subscripts

e	external
h	hydraulic
i	internal
in	inlet
r	refrigerant
sat	saturation
w	water, coolant
wall	wall

small heat transfer rates, coupled with the high heat transfer coefficients in these minichannels, require the deduction of heat transfer coefficients based on small saturation to wall temperature differences.

Most of the condensation data available were taken in multiport minichannels and were measured with the Wilson plot technique that allows calculating the inner heat transfer coefficient from the difference between the total and the external heat transfer resistance. The main shortcoming of this method, which on the other hand does not require the measurement of the wall temperature, is the high experimental uncertainty for the heat transfer coefficients particularly when the leading thermal resistance is on the coolant side. Furthermore, in the case of multiport tubes, the heat transfer coefficient measured with the indirect experimental method represents only an average value over the parallel channels and does not give appropriate information for the single channels. Besides, in the case of small cross-flow area, it becomes very difficult to reduce the vapour quality change in the test section and therefore, for most experimental data, it is impossible to get local or quasi local values of the heat transfer coefficient.

The present paper aims to provide an experimental technique which allows the measurement of local heat transfer coefficients in a single minichannel.

A new experimental setup for the measurement of heat transfer coefficient and pressure drop during condensation inside a single minichannel test tube is presented. The test section has been designed so as to measure local heat transfer coefficients and to reduce the nominal experimental uncertainty associated with the measuring technique. In comparison to the case of multiport tubes, averaged values over a number of parallel channels are here substituted with the heat transfer coefficient in one single channel obtained through the measurement of the heat flux and the saturation minus wall temperature difference.

Besides, the local values of the heat transfer coefficient measured with R134a and R32, fluids displaying far different reduced pressure, are presented in the paper and are used to validate available correlations for condensation heat transfer coefficient.

2. Short literature review

One of the first review about condensation inside minichannels was provided by Cavallini [2] and later updated by Cavallini et al. [3], covering flow regimes, pressure drop and heat transfer modelling. The condensation mechanisms in minichannels have also been extensively treated by Garimella [4].

As reported in Cavallini et al. [3], several researchers measured the heat transfer coefficient during condensation of refrigerants in small diameter tubes. Most of the available experimental data refer to one fluid only, namely R134a. Some tests were also performed with R11, R12, R22, R123, R410A, R236ea; few data points are available for R407C, and more recently the fluids R245fa and HFE7100 have also been tested.

Most data were measured in multiport channels and were collected with the Wilson plot technique. As already observed, this method gives quite high uncertainty values for the heat transfer coefficients. In some of the most recent papers original measurement techniques are presented. Yang and Webb [5], Zhang and Webb [6], Webb and Ermis [7], Yan and Lin [8] and Vardhan and Dunn [9] measured the heat transfer coefficient during condensation of refrigerants inside small diameter tubes or minichannels, both plain and microfinned. Also recently Wang et al. [10], Garimella [11], Kim et al. [12], Koyama et al. [14] and Baird et al. [15] collected experimental heat transfer coefficient data for condensation in minichannels. All the experiments were referred to mass velocities higher than 70 kg m^{-2} s^{-1}. Recently Cavallini et al. [16] measured data relative to the fluids R236ea, R410A, R134a, condensing at 40 °C in a multiport minichannel. These data have been measured with an accuracy of ±7% at typical test conditions.

Wang et al. [10] measured heat transfer coefficients during condensation of R134a inside an air cooled horizontal multiport aluminum condenser with 1.46 mm hydraulic diameter channels. The authors used thermocouples to measure the external surface temperature.

Koyama et al. [14] tested four multiport extruded tubes with and without microfins during condensation of R134a at around 60 °C inlet saturation temperature. They inserted heat flux sensors between the water jackets and the test tube and measured the outer wall temperature of the test tube with buried T-type thermocouples.

Garimella [11] developed a thermal amplification technique with a primary high flow rate coolant loop and a secondary low flow rate coolant loop. In this way he could apply the Wilson plot technique with a high refrigerant side to coolant side resistance ratio. At the same time he could measure the heat duty with low uncertainties even at low heat transfer rates. He measured heat transfer coefficients during condensation of R134a in a square channel 0.76 mm in hydraulic diameter.

Baird et al. [15] measured heat transfer coefficients during condensation of R11 and R123 in 0.92 and 1.95 mm internal diameters tubes with thermoelectric coolers as heat sinks. The tube was inserted in a copper block and the wall temperature was assumed to be equal to the measured block temperature. Thermal contact resistance was measured and found to be negligible.

Kim et al. [13] presented experimental heat transfer coefficients measured during condensation of R134a in a horizontal single round tube with an inner diameter of 0.691 mm. They developed an original experimental technique. The test tube

and an additional tube were both laid in the same air flow: the refrigerant flowed into the test tube, while a heater wire was inserted into the other tube. The authors estimated the heat flow rate dissipated by the condenser from the power input of the heater tube when wall temperatures of the two samples had reached the same values. Indeed, six T-type thermocouples were soldered onto the outer surface of the test tube to measure the tube surface temperatures.

In Bandhauer et al. [17] measurements during condensation inside channels with 1.5 mm > d_h > 0.5 mm are reported. In their apparatus, they use the already mentioned so-called thermal amplification technique: the test section is cooled using water at a high flow rate to ensure that the condensation side displays the governing thermal resistance. Heat exchange with a secondary cooling water stream at a much lower flow rate is used to obtain a large temperature difference, which is used to measure the condensation duty. The authors present a representative case for a channel with d_h = 0.76 mm in which the refrigerant side thermal resistance is much higher than the coolant side thermal resistance. This ensures that the condensation side presents the governing resistance. For the range of mass fluxes investigated, the resistance ratio was between 5 and 29. For a set of data points shown, the average uncertainty in the local heat transfer coefficients was ±21%.

Average heat transfer coefficients were measured with R134a and R245fa condensing in a single rectangular minichannel by Baummer et al. [18]. They also measured the average heat transfer coefficient of R245fa and HFE7100 in a microgroove condenser, covering mass velocity values up to 25 kg m^{-2} s^{-1}.

Some reviews of correlations available in the literature (Cavallini et al. [3], Kandlikar et al. [4]) report comparisons of experimental data with predicting models, both correlations for macroscale condensation and correlations developed for minichannels. Nonetheless, there is not an established predicting model for condensation inside minichannels, mostly because it has not still been explained to what extent the condensation phenomenon inside minichannels differs from macroscale condensation. Besides, the influence of the surface tension on the heat transfer coefficient has not been experimentally quantified and the effect of the cross-section shape of the minichannel is still unclear.

The main purpose of the present work is to obtain accurate microscale local heat transfer data, which can be easily compared to macroscale databases, to measure possible differences among the two processes, if it is the case.

3. Experimental apparatus

3.1. Test rig

The test rig used is depicted in Fig. 1. It consists of the primary (refrigerant) loop and of three auxiliary loops: two cooling water loops and one hot water loop. The subcooled refrigerant from the post-condenser is sent through a mechanical filter and a dehumidifier into an independently controlled gear pump, which is magnetically coupled to a variable speed electric motor.

When the test apparatus is operated for condensation measurements, the fluid is pumped through the Coriolis-effect mass flow meter into the evaporator where the refrigerant is vaporised and superheated in a tube-in-tube heat exchanger. The superheated vapour enters the test section, which is made of two counter-flow heat exchangers: the first one (desuperheater) is used to achieve saturation conditions, the second one is the actual measuring sector.

The pressure is gauged through two digital strain gauge pressure (relative and differential) transducers, connected to manometric taps to measure the fluid pressure upstream and downstream of the test tube.

Two thermal baths are used in the condensation tests: the first one provides the water entering the measuring sector and the desuperheater at a desired temperature, the other one provides the coolant for the post-condenser. When necessary, the cooling water entering the pre-section can be maintained at a higher temperature through an electrical heater installed between the thermal bath and the desuperheater.

The cooling water flow rates, in the pre-section and in the measuring section, are measured by means of two Coriolis-effect mass flow meters and the total temperature gains of the water across both sectors are measured with two copper-constantan four and three-junction thermopiles.

3.2. Test section

For the determination of the local heat transfer coefficient, three parameters are required: the local heat flux, the saturation temperature and the wall temperature. The heat flux is determined from the temperature profile of the coolant in the measuring sector. The vapour temperature in the test section is measured by means of a T-type thermocouple and a three-junction thermopile, which are soldered to the stainless steel capillary tube in the adiabatic sectors, before and after the measuring sector. The presence of both temperature and pressure sensors at the inlet of the measuring sector allows

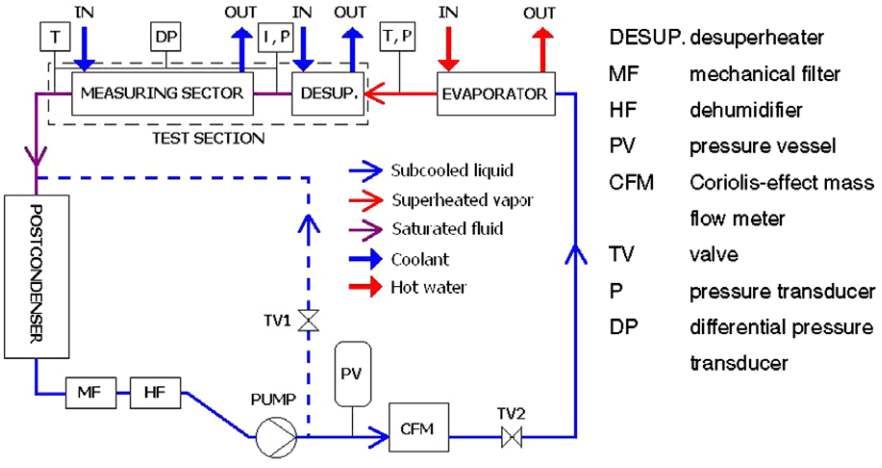

Fig. 1. Experimental test rig.

a double check of the saturation temperature. The tube wall temperature is directly measured, so as to obtain the saturation to wall temperature difference and thus the internal heat transfer coefficient.

The test section is made of two parts: a 0.05 m long pre-section, which works as the desuperheater, and the effective measuring section (0.23 m long); a picture is reported in Fig. 2. Both the pre-section and the measuring sector are shaped as counter-current heat exchangers of similar geometry, with the condensing fluid flowing in the inside channel, and the cooling water flowing in the external channel. The two sectors are connected by a stainless steel capillary tube (adiabatic sector); a similar tube connects the exit of the measuring sector, as depicted in Fig. 3.

The cores of both the desuperheater and the measuring sector are obtained by proper machining the thick wall of a copper tube for industrial application, with internal diameter $d_i = 0.96$ mm and external original diameter $d_e = 8$ mm. The geometry thus obtained for the external coolant channel is illustrated in Fig. 4. The definition of this optimal coolant flow passage geometry has been the first step in the design process of the new test section; this unique geometry increases the external heat transfer area, thus drastically decreasing the related heat transfer resistance. Furthermore the complex flow passage causes throughout local mixing of the coolant in the channel; by changing continuously the flow direction and disturbing the boundary layer. High heat transfer coefficients are thus obtained even at moderate mass flow rates (beneficial for precise heat flux measurements); besides, perfect local mixing of the coolant is a necessary condition to link the temperature variation along the coolant flow to the heat flow rate transferred.

The test section is designed for measurement of local two-phase heat transfer coefficients by measuring the local wall temperature and the coolant temperature profile along the measuring sector, which is used to calculate the local heat flux. The condensing fluid temperature and pressure are directly measured in the adiabatic segments at the inlet and at the outlet to the test tube. The saturation temperature profile is finally obtained from the pressure distribution, which accounts for the effect of frictional, local and momentum pressure change along the sector. Furthermore, the saturation temperature profile is calculated so as to coincide with the two measured values upstream and downstream of the measuring sector.

The number of temperature sensors installed in the measuring sector comes up as a compromise between an appropriate temperature profile description and a feasible design. As a result of CFD modelling and prototype testing, 15 thermocouples have been installed in the coolant channel and 13 thermocouples have been embedded in the wall.

The thermocouples embedded in the wall are installed in 0.6 mm diameter cylindrical holes, machined 0.5 mm far from the internal tube surface (Fig. 5). A numerical analysis was conducted to verify the temperature profile in the copper and to verify if a correction is required for the wall temperature measurement due to the distance between the thermocouple and the inner tube surface. The numerical analysis carried out with the CFD commercial code Fluent resulted in a test condition-dependent temperature difference between the inner surface temperature and the thermocouple location. In the case studied in Fig. 5, the temperature difference between inner surface and thermocouple location is 0.21 K, while the saturation minus wall temperature difference is equal to 13 K, which means that the experimental error due to the thermocouple location is in the order of 1.6%. Nevertheless, this correction is approximately accounted for by calculating the conductive thermal resistance of the copper cylindrical layer between inner tube surface and the thermocouple.

Two stainless steel capillary tubes are soldered to the measuring sector at the two sides. The stainless steel capillary tubes have three major roles. They are used to achieve thermal separation between the desuperheater and the measuring sector and between the measuring sector and the outlet to the test section. They also provide adiabatic sectors where measurement of the saturation temperature of the fluid can be done with a good accuracy on the outer tube surface. The minimum length of stainless steel tube that can offer reliable saturation temperature measurement has been calculated to be around 20 mm.

The third role for the stainless steel tubes is the accommodation of the pressure ports. A numerical study has been performed to check the effect of the pressure lines (working as fins) on the adiabatic tube. The thermal disturbance of the pressure lines has a negligible influence on the adiabatic wall surface temperature measurement. The adiabatic sector is 31 mm long: the thermocouple is located at 12 mm far from the measuring sector edge of the adiabatic capillary tube, being the pressure port 23 mm far from the same edge.

So far, the present test section represents a unique experimental apparatus for condensation inside minichannels and its advantages can be schematically summarized as follows:

- it facilitates accurate measurement of local "quasi-mixing cup" temperatures of the water at low flow rates permitting evaluation of the local heat fluxes;
- it provides improved precision in the evaluation of condensation heat transfer coefficients owing to the large ratio of heat transfer surface areas;
- it allows the insertion of many wall thermocouples without passing through the cooling water, minimizing error due to conduction along the thermocouple wires, and due to spurious emf's build up for the presence of high temperature gradients in the thermocouples wires.

4. Experimental technique

4.1. Data reduction

Fig. 6 displays saturation, wall and water temperatures for a test run at 600 kg m^{-2} s^{-1} mass velocity with R134a. The same graph reports the saturation temperature obtained from the pressure transducers and the temperature directly measured in the adiabatic walls upstream and downstream of the condensa-

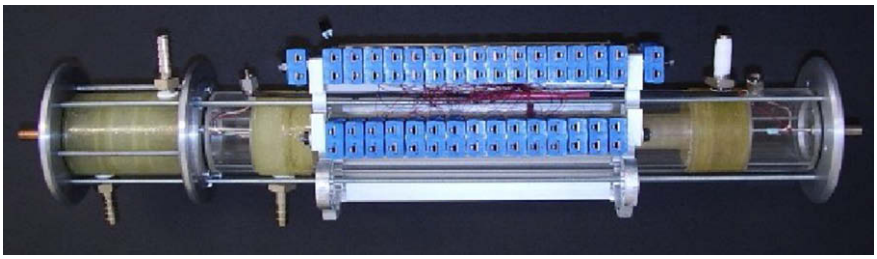

Fig. 2. Picture of the circular minichannel test section.

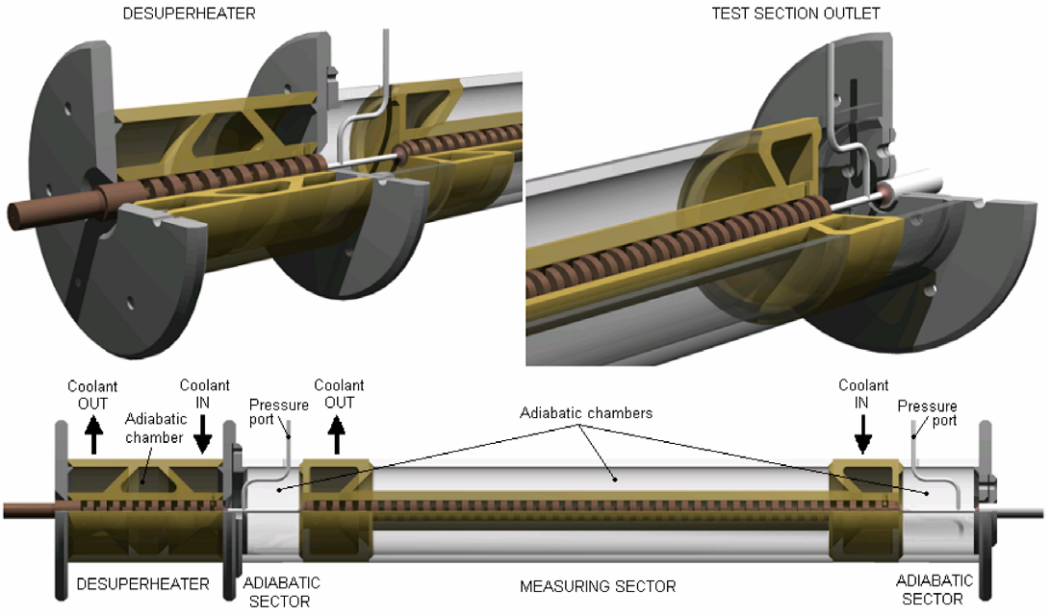

Fig. 3. View of the new test section for circular minichannel.

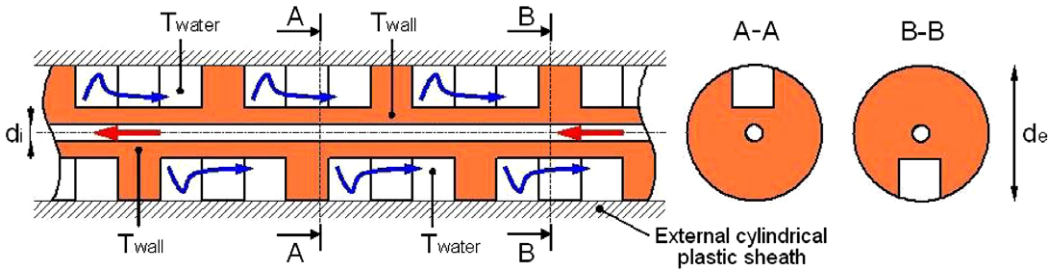

Fig. 4. Details of the coolant flow passage geometry.

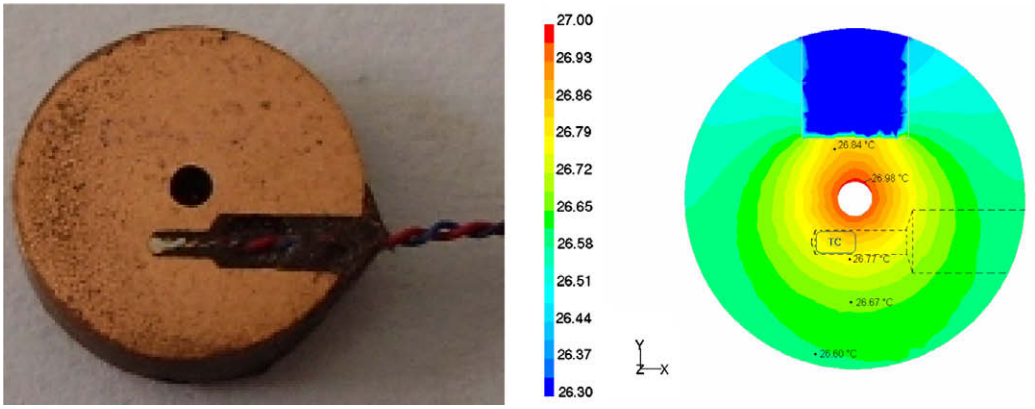

Fig. 5. (Left) Enlarged image of the cross-section of the fin sample where the wall temperature is measured. Junction of the TC is electrically insulated and is glued in its position with high thermally conductive glue. (Right) Contours of wall temperature around the thermocouple in the copper tube.

tion length. With respect to the water temperature measured along the channel, the slope of the profile is used to calculate the local heat flux:

$$q' = -\dot{m}_w \cdot c_{pw} \cdot \frac{1}{\pi \cdot d_i} \cdot \frac{dT_w(z)}{dz} \quad (1)$$

where z is the axial coordinate along the tube oriented with the refrigerant flow and dT_w/dz is the derivative of the polynomial equation interpolating the water temperature along z. Similarly, it is possible to calculate the derivative of the equation interpolating the wall temperature, which provides information about the axial conduction along the channel. Fig. 7 shows both the derivative of water and wall temperatures for the above test run.

The local heat transfer coefficient inside the minichannel can be obtained as the ratio of heat flux to saturation minus wall temperature difference:

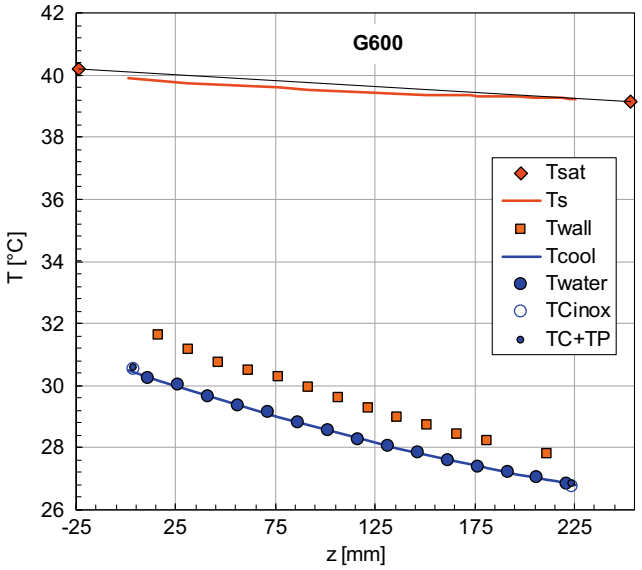

Fig. 6. Refrigerant, wall and coolant temperature measurements with R134a at $G = 600\ \mathrm{kg\ m^{-2}\ s^{-1}}$ along the measuring sector. Symbols refer to local temperature measurements.

$$\alpha_i(z) = \frac{q'(z)}{[T_{sat}(z) - T_{wall}(z)]} \tag{2}$$

It should be pointed out here that the saturation temperature is known only at the inlet and outlet to the measuring sector, from the saturation pressure measurements.

Since the difference of saturation minus wall temperature is pretty large for typical test conditions and the saturation temperature drop due to pressure drop is rather small (see Fig. 6), for most of the test conditions the saturation temperature along the channel can be derived as a linear trend from the two known values without making a significant error on the heat transfer coefficient. As a matter of fact, the vapour quality changes during the condensation process and therefore the pressure gradient varies along the channel. Fig. 8 shows two curves of the saturation temperature profile: a linear trend between inlet and outlet and a second curve obtained by matching a pressure drop curve to the measured values at the inlet and at the outlet.

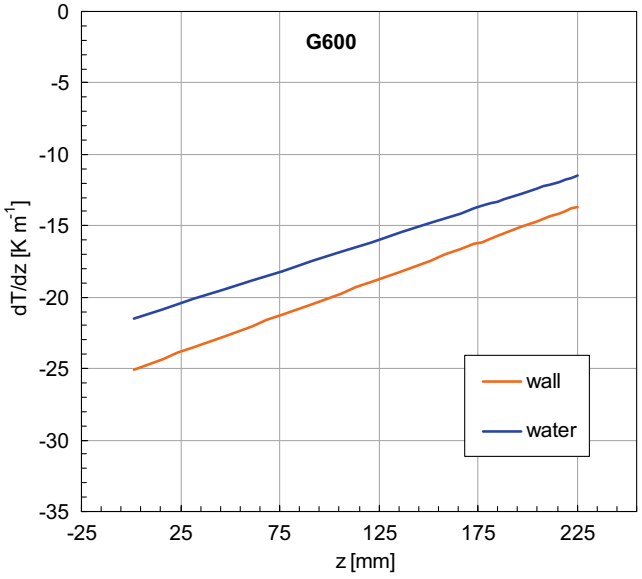

Fig. 7. Coolant and wall temperature gradient profiles along the measuring sector at 600 kg m^{-2} s^{-1} mass velocity with R134a.

The resulting temperature profile is obtained from the equation of frictional pressure gradient by Friedel [19] and the momentum component with the Rouhani and Axelsson [20] void fraction. The last curve is the one used in the data reduction of the present tests. However, for most test conditions, there is no appreciable difference on the heat transfer coefficient from using the two different curves of saturation temperature.

The outlet saturation temperature is obtained by subtracting from the inlet temperature the saturation temperature drop. This temperature drop is obtained by means of a differential pressure transducer and it is checked by using a copper-constantan thermopile between inlet and outlet. Since subcooled refrigerant could be present at the outlet, the outlet saturation temperature used in the present data reduction is determined from the measured pressure drop.

The heat flow rate transferred to the secondary fluid up to a certain position z is obtained by integrating the local heat flux q' from 0 (refrigerant inlet) to z.

$$q(z) = \pi \cdot d_i \cdot \int_0^z q'(z)\mathrm{d}z \tag{3}$$

The local thermodynamic vapour quality at any location z can be found from the heat flow rate, the mass flow rate, the latent heat and the inlet vapour quality:

$$x(z) = x_{in} - \frac{q(z)}{\dot{m}_r \cdot h_{LG}} \tag{4}$$

The vapour quality at the inlet to the measuring sector x_{in} is obtained from the energy balance on the coolant side of the desuperheater. In fact, the specific enthalpy of the superheated refrigerant at the inlet to the pre-section is known from the local pressure and temperature. The enthalpy variation in the desuperheater is obtained from the heat flow rate transferred in the desuperheater and, in turn, this enthalpy change is used to calculate the vapour quality at the inlet to the measuring sector.

Fig. 9 displays the heat transfer coefficient and the vapour quality for the test run with R134a at 600 kg m^{-2} s^{-1} mass velocity along the channel.

4.2. Calibration procedure and error analysis

In the calibration of the system there are some actions that are regularly performed to assure the accuracy of the measurements:

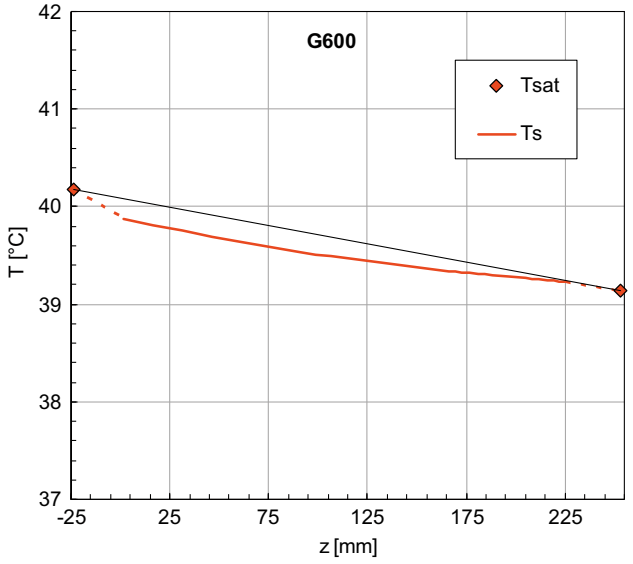

Fig. 8. R134a saturation temperature profiles used in the determination of the heat transfer coefficient.

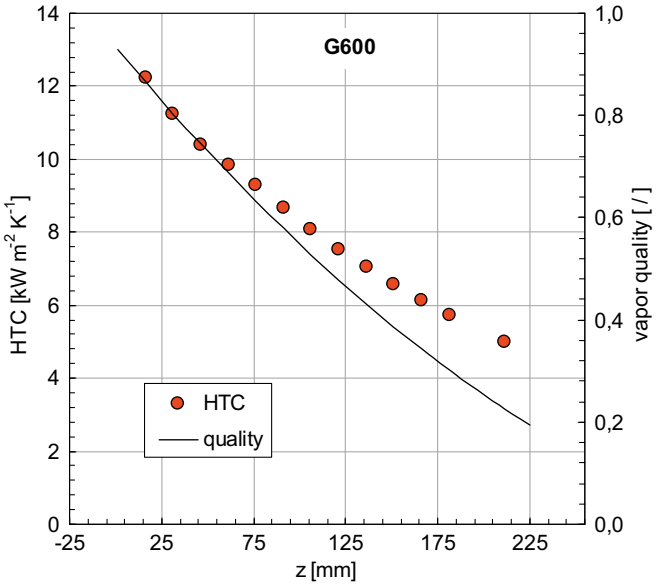

Fig. 9. R134a experimental HTC and vapour quality versus axial position for condensing flow at 600 kg m^{-2} s^{-1} and 40 °C saturation temperature inside the minichannel.

on-site calibration of the thermocouples,
check of temperature and pressure under saturated conditions,
check of thermal balance in the test section and in the measuring sector.

The experimental uncertainties for the measured parameters are reported in Table 1. In the case of thermocouples, the reported uncertainty comes from the off-site calibration tests. However, a different successive on-site calibration of the thermocouples installed in the wall and in the water channel has been performed and later repeated on a regular basis, especially with regards to the temperature difference among them. This on-site calibration is performed by circulating water under constant and adiabatic conditions in the channel and using a calibrated thermistor probe Pt100 as the reference thermometer. A correction function for each thermocouple is determined from the on-site calibration procedure. The range of variation of the water and the wall thermocouples readings from the calibration vary within ±0.01 K of the reference temperature.

As an important check of the experimental apparatus, the refrigerant temperature at inlet to the measuring sector is also measured by means of a copper-constantan thermocouple. This temperature is compared to the saturation temperature obtained from the pressure: the disagreement is typically below 0.15 K, which is within the uncertainty range of the two instruments. This check shows that no subcooled liquid flows at the wall in the adiabatic segments due to condensation in the pre-section.

The energy balance in the test section is checked by comparing the water side heat flow rate with the one calculated on the refrigerant side when superheated vapour enters the test section and subcooled liquid exits.

Besides, a check on the integrated local heat flux is regularly performed. The total heat flow rate in the measuring sector is calculated by integrating the heat flux between 0 and L, where L is the length of the measuring sector, and verified from the overall cooling water temperature gain measured with a three junction copper-constantan thermopile:

$$q_{\text{tot}} = \pi \cdot d_{\text{i}} \cdot \int_0^z q'(z)\mathrm{d}z = \dot{m}_{\text{w}} \cdot c_{p\text{w}} \cdot \Delta T_{\text{w}} \tag{5}$$

In all tests presented here, there is a disagreement below 3% between the two methods in Eq. (5).

Prior to collecting measurements, an ad-hoc investigation on the influence of the ambient temperature on measurements has been performed. Since the total heat flow rate in the pre-section or in the measuring sector may be pretty low at certain operating conditions, after properly insulating the test section, some tests have been performed to check the heat transfer between the water and the ambient air at varying water-to-air temperature difference. This heat dissipation was found to be negligible at medium and high refrigerant mass velocities, while at the lowest tested mass velocity a proper correction was accounted for the effect of the ambient heat dissipation on the heat transfer coefficient and the vapour quality.

As a phase change process is usually associated with high heat transfer coefficients, low temperature differences between the wall and the condensing fluid usually represents a major reason of nominal experimental error. The low experimental uncertainty which can be achieved with the present experimental technique is partly due to the particular geometry of the coolant channel which reduces the thermal resistance on the coolant side, both because of the high external heat transfer coefficient and because of the external enhanced surface area. In fact, the ratio of the thermal resistance of the refrigerant side to that of the coolant side is typically around 6, which ensures that the condensation side presents the governing resistance. As a consequence, the uncertainty associated with the calculated heat transfer coefficient is dominated by the uncertainty in the heat flux, which in turn depends on the uncertainty of the cooling water temperature profile.

The nominal experimental uncertainty of the local heat transfer coefficient measurement was calculated from Eq. (6). The uncertainty contributions were calculated for the four main actors associated to the heat transfer coefficient measurement.

Table 1
Experimental uncertainty for measured parameters.

Temperature	±0.05 K
Temperature difference (with thermopile)	±0.03 K
Water flow rate	±0.2%
Refrigerant flow rate	±0.2%
Absolute pressure	±3 kPa
Pressure difference	±0.1 kPa

$$\delta_{\alpha(z)} = \sqrt{\left(\frac{\alpha(z)}{\dot{m}_{\text{w}}}\cdot\delta_{\dot{m}_{\text{w}}}\right)^2 + \left(\frac{\alpha(z)}{T'_{\text{w}}(z)}\cdot\delta_{T'_{\text{w}}}\right)^2 + \left(\frac{\alpha(z)}{\Delta T_{\text{ref-wall}}(z)}\cdot\delta_{\Delta T_{\text{ref-wall}}}\right)^2 + \left(\frac{\alpha(z)}{d_{\text{h}}}\cdot\delta_{d_{\text{h}}}\right)^2} \tag{6}$$

The relative contributions to the overall experimental uncertainty due to mass flow rate measurements and hydraulic diameter remain rather constant for the entire span of mass velocities and vapour qualities. Relative contributions due to the wall-to-saturation temperature difference and temperature gradient measurement on the other hand depend on refrigerant and coolant mass flow rate, vapour quality and also on coolant temperature. The highest uncertainty value in this particular case is associated to the lowest refrigerant mass velocity and the lowest vapour quality.

In the case of R134a, the overall calculated relative uncertainty is rather constant in the entire vapour quality span for high refrigerant mass velocities. Fig. 10 shows the relative percentage uncertainty of the heat transfer coefficient and the uncertainty components to the total value at 1200 kg m^{-2} s^{-1}. The overall uncertainty is always below 5%, for the entire range of vapour quality, down to 4.3% at 0.88 vapour quality. Similar values are found at 1000 kg m^{-2} s^{-1}, with the highest nominal accuracy of 4.5% calculated at 92% vapour quality.

The lower the mass velocity, the higher the experimental uncertainty. At 800 kg m^{-2} s^{-1}, it is always below 6%, while at 400 kg m^{-2} s^{-1} it ranges between 5% and 10%.

As it can be seen from Fig. 11, where the uncertainty is plotted for tests at 200 kg m^{-2} s^{-1}, the uncertainty associated to the heat flux obtained from the water temperature gradient is far away the larger uncertainty component and it varies a lot when moving from 1 to 0 vapour quality. At 0.9 vapour quality the overall uncertainty is equal to 6% while it exceeds 16% at 0.14 vapour quality.

Similarly, but with a worst result in terms of accuracy, at 100 kg m^{-2} s^{-1} the overall relative uncertainty increases when decreasing the vapour quality, rising from 12% at 0.85 vapour quality up to 27% at $x = 0.12$.

4.3. Single phase friction factor and heat transfer coefficient

Prior to any two-phase measurement, some tests with single phase R134a fluid flowing in the test section have been carried out.

The friction factor has been measured during adiabatic flow of subcooled liquid and superheated vapour. The internal surface roughness of the channel was measured finding an average roughness equal to 1.3 μm. The measured friction factor has found to be in good agreement with the Hagen–Poiseuille correlation in the laminar flow, while in the turbulent flow region it follows the Churcill correlation by using the measured value of roughness in the model. More details are reported in Cavallini et al. [21].

The heat transfer tests have been performed with subcooled liquid, both in the heating and cooling mode. The Reynolds number was varied between 3000 and 8000 and the heat transfer coefficient was compared against the correlations reported in VDI [22] and [23]. As it can be seen in Fig. 12, for the high values of HTC

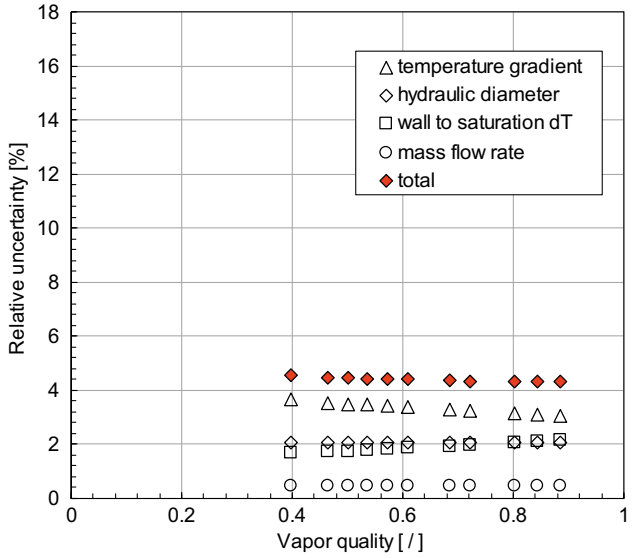

Fig. 10. Calculated absolute values for the four main contributions of the experimental heat transfer coefficient uncertainty versus vapour quality at 1200 kg m^{-2} s^{-1} mass velocity of R134a.

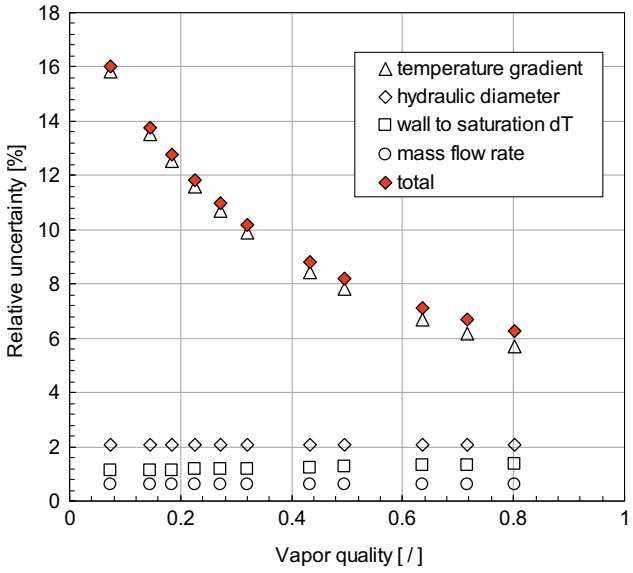

Fig. 11. Calculated absolute values for the four main contributions of the experimental heat transfer coefficient uncertainty versus vapour quality at 200 kg m^{-2} s^{-1} mass velocity of R134a.

at Reynolds number above 5000, closer to the turbulent region, the measured heat transfer coefficient is predicted by the correlations within ±10%, while at lower Reynolds number the two models give different predicted values.

4.4. Sensitivity to inlet vapour conditions

Since the purpose of the present apparatus is to accurately measure the local heat transfer coefficient, several tests have been performed to check the technique.

Fig. 13 shows the experimental heat transfer coefficient measured with R32 at 600 kg m^{-2} s^{-1} by imposing different inlet conditions to the refrigerant entering the test section. In the test runs, the refrigerant has been first sent as superheated vapour to the measuring sector, and then at lower and lower values of vapour quality, down to 78% quality. The local heat transfer coefficient determined in the different test runs perfectly overlap, as it can be seen in Fig. 13. That is, the present test apparatus provides exactly the same value of the heat transfer coefficient at the same refrigerant conditions, no matter which location this coefficient is measured at along the channel.

4.5. Sensitivity to coolant conditions

As previously demonstrated, the uncertainty in the coolant temperature profile is the major contribution to the overall uncertainty in the present experimental technique. For this reason, it is absolutely important that the water temperature be accurately measured along the channel. As an indirect validation of the present technique, it was checked that the coolant operating conditions does not affect the resultant internal heat transfer coefficient, provided that the refrigerant conditions are maintained fixed.

Fig. 14 shows the measured heat transfer coefficient of R134a condensing at 417 kg m^{-2} s^{-1} mass velocity and 40 °C saturation temperature in the channel. The coolant mass flow rate was varied between 10 and 20 kg/h and no effect on the internal heat transfer coefficient was detected.

Fig. 15 shows the R134a heat transfer coefficient measured at the same refrigerant conditions ($G = 417$ kg m^{-2} s^{-1}, $T_{sat} = 40$ °C) when the coolant flow rate was maintained fixed but the inlet cool-

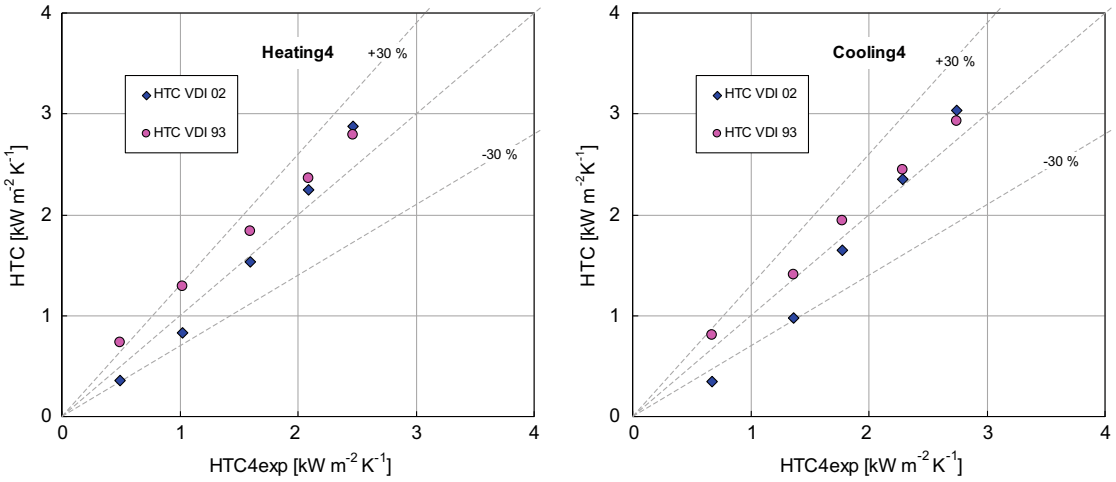

Fig. 12. Experimental heat transfer coefficients measured during R134a single phase flow and compared against correlations for forced convective heat transfer.

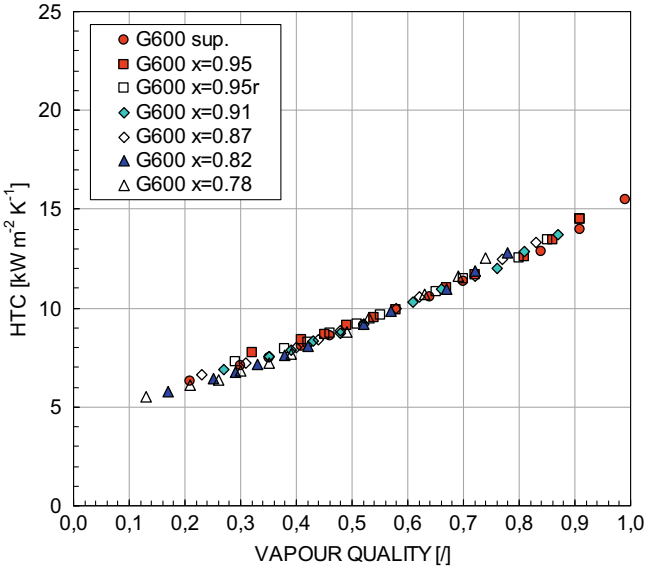

Fig. 13. Experimental local heat transfer coefficient versus vapour quality for R32 at different inlet vapour conditions ranging from superheating to 0.78 quality.

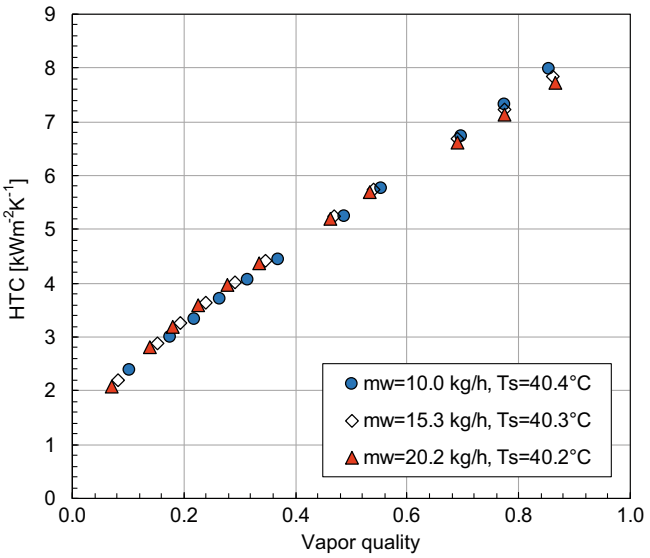

Fig. 14. Experimental local heat transfer coefficient versus vapour quality for R134a at variable water flow rates.

ant temperature was varied from 15 to 29 °C. Since the inlet refrigerant conditions do not change, the variation of the coolant temperature implies a change in the saturation to wall temperature difference. From previous investigations of condensation in macroscale tubes, it is well known that no effect of the saturation to wall temperature difference on the heat transfer coefficient is to be expected when the annular flow is established in the tube. Cavallini et al. [24] found no effect of the temperature difference with R134a condensing at 400 kg m^{-2} s^{-1} mass velocity in an 8 mm tube and this result can easily be transferred to the present minichannel, where the annular flow is expected to establish at even lower mass velocity. Fig. 15 shows that no effect of the inlet coolant temperature is measured on the heat transfer coefficient and this may be looked at as an additional assessment of the present experimental technique.

Such a study has also been conducted for R32 flowing at 200 kg m^{-2} s^{-1} mass velocity, with coolant inlet temperature ranging between 19 and 29 °C. As previously mentioned, these variations of the coolant temperature imply a consequent significant change in the wall temperature and thus in the saturation to wall temperature difference. The results are plotted in Fig. 16, showing no effect of the temperature difference on the heat transfer coefficient. These results confirm that the effect of gravity in an around 1 mm diameter channel is not significant in comparison with the other forces influencing the condensation heat transfer even at 200 kg m^{-2} s^{-1} mass velocity.

5. Experimental results

Fig. 17 reports the experimental heat transfer coefficients measured during condensation of R134a at 40 °C saturation temperature, correspondent to 1017 kPa saturation pressure. Fig. 18 shows the heat transfer coefficient measured with R32 at the same saturation temperature, which corresponds in this case to the pressure of 2478 kPa. For both fluids, the database depicted in the figure covers mass velocities from 100 up to 1200 kg m^{-2} s^{-1} over the entire range of vapour quality.

The experimental values of the heat transfer coefficient were determined as the ratio of heat flux to saturation minus wall temperature difference. Each dot in the diagram is obtained from a

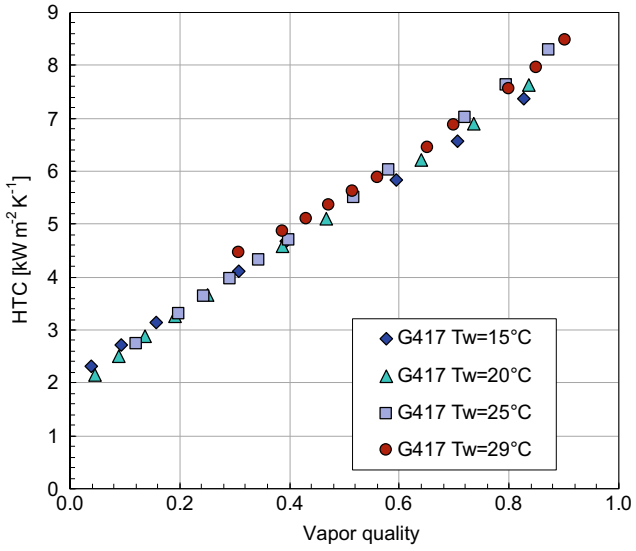

Fig. 15. Experimental local heat transfer coefficient versus vapour quality for R134a at variable inlet water temperatures.

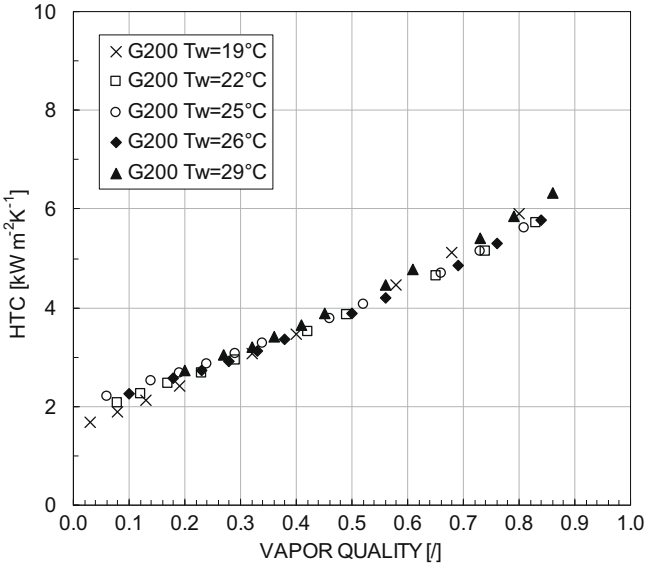

Fig. 16. Experimental local heat transfer coefficient versus vapour quality for R32 at variable inlet water temperatures.

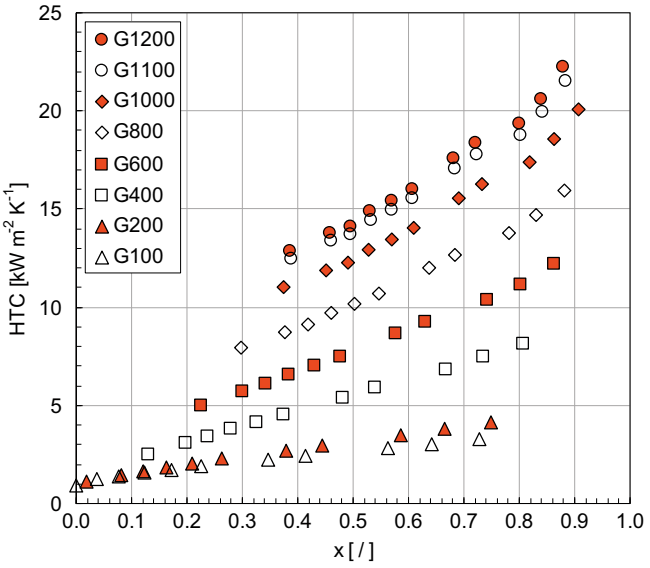

Fig. 17. Local experimental condensation heat transfer coefficient versus vapour quality for R134a at mass velocities ranging from 100 to 1200 kg m^{-2} s^{-1}.

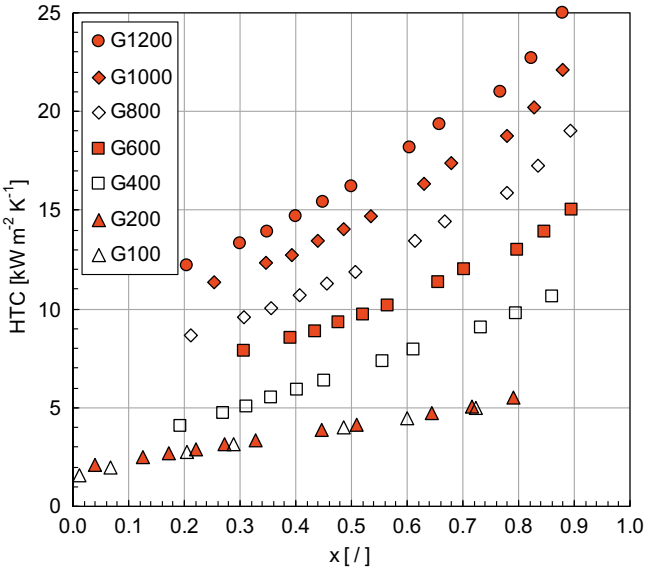

Fig. 18. Local experimental condensation heat transfer coefficient versus vapour quality for R32 at mass velocities ranging from 100 to 1200 kg m^{-2} s^{-1}.

wall temperature reading: the first and the last temperature readings in the wall seem to be affected by axial boundary effects and therefore those two readings are not used for the determination of the heat transfer coefficient.

As shown in Figs. 17 and 18, the heat transfer coefficients display the usual trend that one would expect for condensation inside plain tubes: the heat transfer coefficient decreases as the condensation proceeds and the vapour quality decreases in the channel. Besides, the heat transfer coefficient increases with mass velocity, implying that condensation must be dominated by shear stress at these operating conditions. As a partial exception to the dominant behaviour, it can be seen that the data points referred to 100 and 200 kg m^{-2} s^{-1} mass velocities almost overlap in the graph of R32 and also in the graph of R134a at least at low quality. This may be due to the effect of other forces acting during condensation, that is the surface tension effect and the gravity force. All the same, one should remember that the nominal uncertainty of the present technique gets the highest at the lowest mass velocity and the heat transfer coefficient measured at 100 kg m^{-2} s^{-1} presents an experimental accuracy between 10% and 25%.

When comparing the heat transfer coefficient of R134a to the one measured for R32, one can see that the latter fluid displays a higher coefficient at the same operating conditions, and this is related to the properties of R32, particularly to the high conductivity of the liquid. At 40 °C, the thermal conductivity of saturated liquid is equal to 74.7 mW m^{-1} K^{-1} for R134a and 114.6 mW m^{-1} K^{-1} for R32.

For the evaluation of working fluids, there is no reason to compare them at the same mass velocity since they may also display different values of pressure drop which means different saturation temperature drop in the heat exchangers. From this point of view, the high pressure fluid R32 performs even additionally better than R134a.

No flow visualisation has been performed during the present work and therefore some clues about the flow regime in the

channel may be obtained by plotting the present data on flow pattern maps. Unfortunately, no general map is available for condensation in minichannels. Figs. 19 and 20 report the present data on the map by Soliman [25] which was developed for macroscale condensation conditions. According to this map, four flow patterns are present during condensation: wavy and intermittent, annular, annular mist and mist flow. A very limited number of points fall in the wavy and intermittent region, while most of the data points, both for R134a and R32, lay in the annular and annular/mist regions.

Fig. 21 depicts the map developed by Coleman and Garimella [26] from visualisation of R134a flowing at 52 °C in a 1 mm diameter channel. The transition curves provided by these authors and reported also in Garimella [4] are not a function of the fluid properties and thus one should not use the map out of the operating conditions reported by the author. Nevertheless, these transition curves may represent an interesting reference for two-phase flow at least for the test runs with R134a, being the saturation temperature pretty close to the one above.

As shown in the map by Garimella, five flow regimes are detected: plug/slug flow, plug/slug and annular film flow, annular film flow, annular and mist flow, mist flow. According to this map, most of the test runs are characterized by plug/slug flow or annular film flow. A bunch of the data fall in the mist flow region. Those data points refer to high vapour quality and high mass velocity.

6. Assessment of predicting correlations

The present database has been compared against some models available in the open literature. The first comparison is shown in Fig. 22, where the predicted heat transfer coefficient is calculated from the model by Moser et al. [27] applied along with the correlation by Zhang and Webb [6] for pressure gradient in small diameter channels. The correlation is able to catch the experimental trend of data, but it underpredicts the data points by 8–25%. The disagreement is higher at the lowest mass velocity and this may be explained by considering that this correlation has been developed for annular flow conditions.

The model by Koyama et al. [14], which was developed for minichannels, is used in the comparison presented in Fig. 23. This model does not give an accurate prediction of the present data, mainly because it is not able to catch the experimental trend of the data versus mass velocity.

Recently, Cavallini et al. [3] developed a new model for forced convective condensation heat transfer prediction inside minichannels. The experimental results relative to shear dominated flow regimes from different authors have been used in the model development. The correlation is based on the Kosky and Staub [28] theoretical analysis that links the heat transfer coefficient to the frictional pressure gradient through the interfacial shear stress. The present correlation also takes into account the liquid entrainment in the gas core, which becomes an important parameter at higher gas velocities, that is higher mass velocities and vapour qualities. The agreement between the present experimental results and calculated values by Cavallini et al. [3] model is good (Fig. 24),

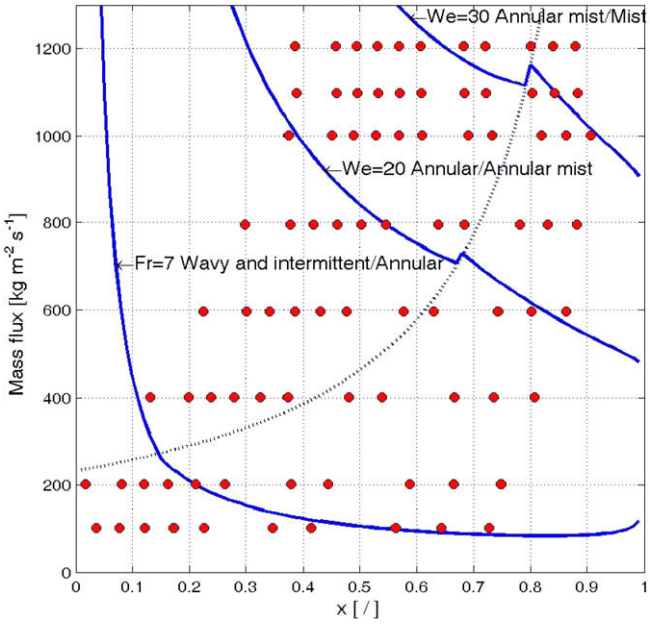

Fig. 19. Flow regime map by Soliman [25] for refrigerant R134a.

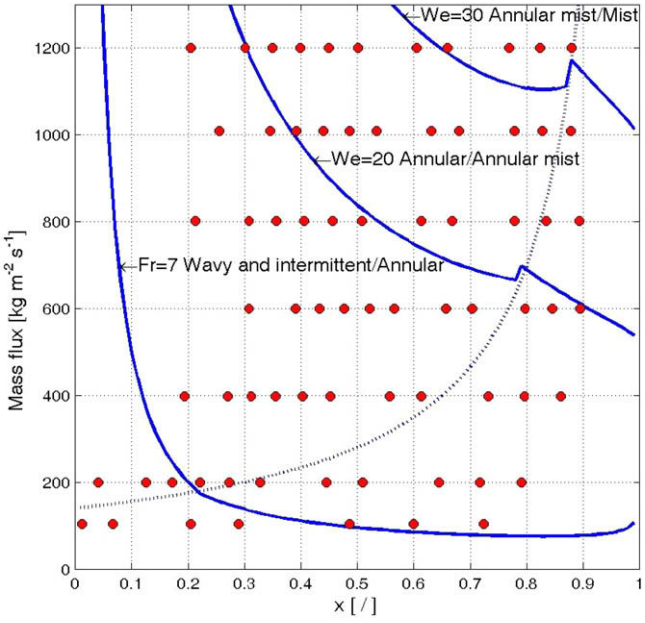

Fig. 20. Flow regime map by Soliman [25] for refrigerant R32.

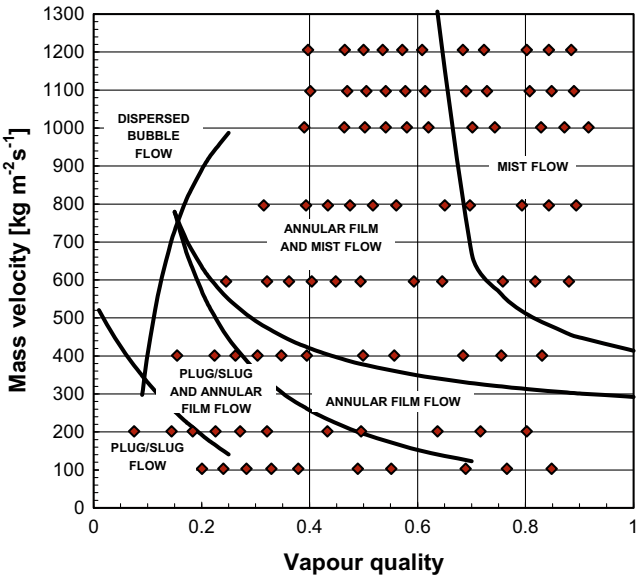

Fig. 21. Flow regime map by Coleman and Garimella [26] and Garimella [4] for R134a.

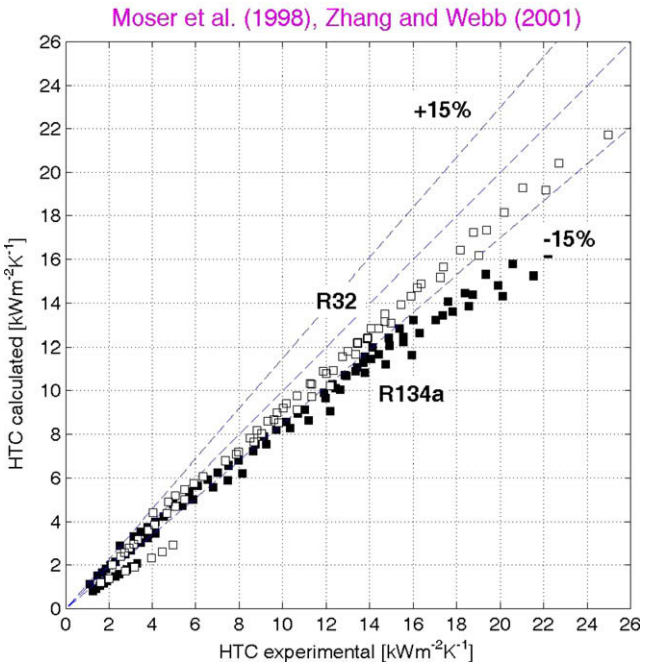

Fig. 22. Comparison between measurements and calculated heat transfer coefficients by Moser et al. [27] as modified by Zhang and Webb [6]. Black symbols refer to R134a, empty symbols to R32.

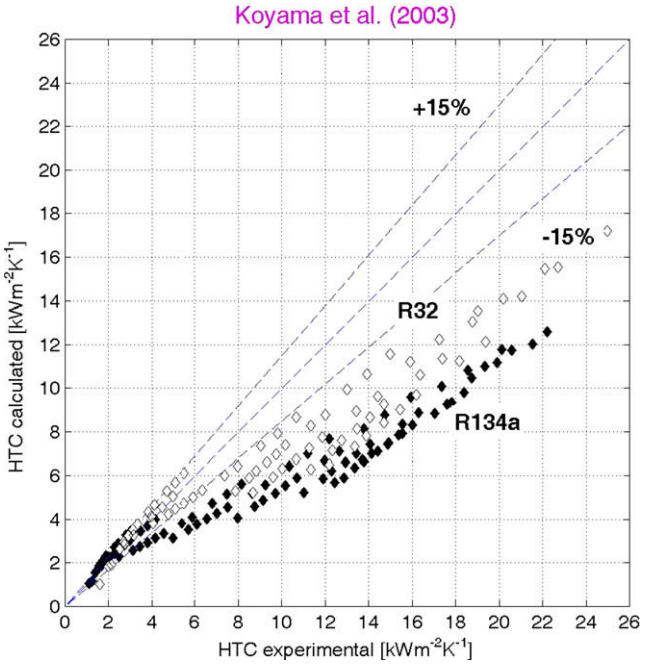

Fig. 23. Comparison between measurements and calculated heat transfer coefficients by Koyama et al. [14]. Black symbols refer to R134a, empty symbols to R32.

although the model overpredicts the highest values of the heat transfer coefficient due to the enhancing effect of the entrainment correlation at these conditions.

The last model compared against the present database is the one by Cavallini et al. [29], which was developed for modelling condensation inside common macroscale plain tubes. This model is a flow regime-based model where all possible operating conditions occurring during condensation in plain tubes are divided in two main regions, depending whether the heat transfer coefficient is ΔT-dependent or ΔT-independent, where ΔT stands for the

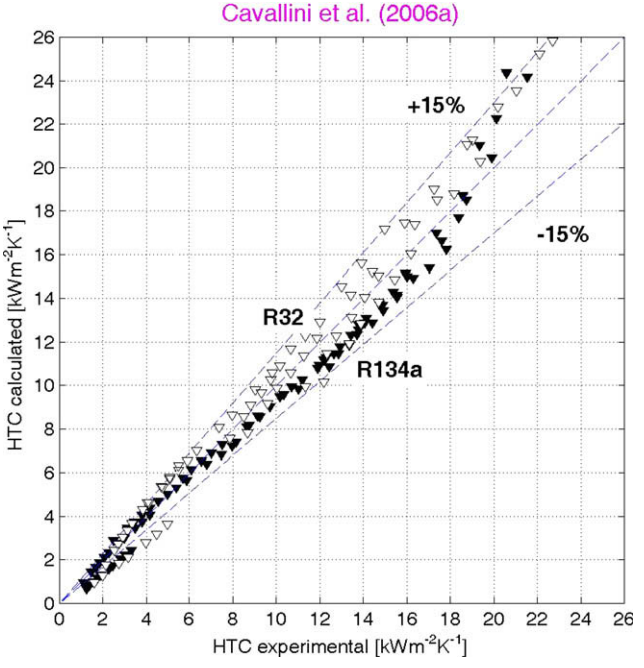

Fig. 24. Comparison between measurements and calculated heat transfer coefficients by Cavallini et al. [3]. Black symbols refer to R134a, empty symbols to R32.

saturation to wall temperature difference in the channel. With regard to the present minichannel database, only very few data points at 100 kg m^{-2} s^{-1} and low vapour quality fall in the ΔT-dependent region. This model, which can pretty easily be implemented and requires a low computational effort, was originally developed from an experimental database gathered by Cavallini et al. [29] inside usual plain tubes, with tube diameter ranging from 3 to 8 mm. Even though the model was not tuned to minichannel heat transfer coefficients, it provides the best predictions of the present data (Fig. 25). Only at the lowest mass velocity the

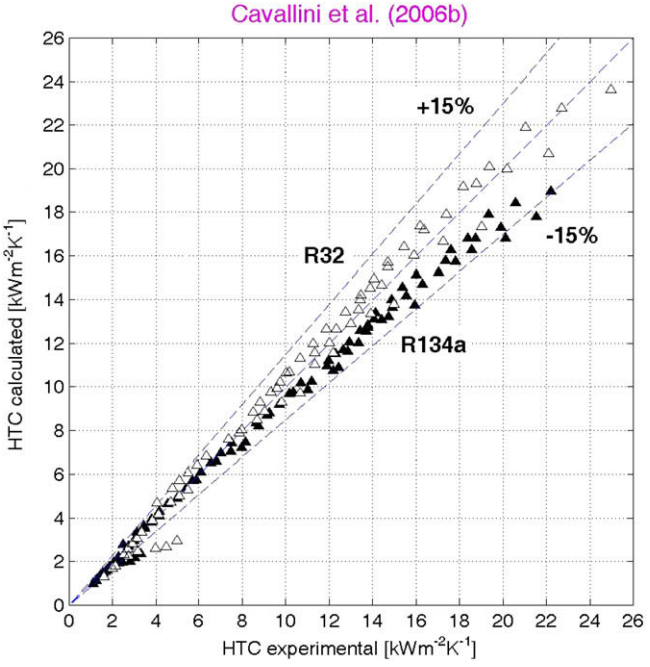

Fig. 25. Comparison between measurements and calculated heat transfer coefficients by Cavallini et al. [29]. Black symbols refer to R134a, empty symbols to R32.

disagreement (underprediction) between calculated and experimental heat transfer coefficient is higher than 15%. This deviation may be related to the different flow patterns occurring in the minichannel at low mass velocity as compared to the macroscale channels.

On the whole, the agreement between experimental results and predictions is good for the last model. In the range 200–1200 kg m^{-2} s^{-1}, the present data show no significant discrepancy from the trend expected in macroscale channels. At the lowest mass velocity, 100 kg m^{-2} s^{-1}, as compared to the macroscale condition, the simultaneous effect of gravity and surface tension in the minichannel may be responsible for a different flow pattern and therefore some change in the heat transfer.

7. Concluding remarks

The present paper reports local heat transfer coefficients during condensation at 40 °C saturation temperature of R134a and R32 in a 0.96 mm diameter circular channel at mass velocity between 100 and 1200 kg m^{-2} s^{-1}.

The experimental technique shown here allows the measurement of the local heat transfer coefficient with high experimental accuracy, since it is obtained from the local heat flux, which in turn comes from the coolant temperature profile. On the whole, more than 30 thermocouples have been installed in the test section, to measure refrigerant, wall and water temperatures.

The experimental trend shows no significant discrepancy from what one would expect for the condensation process by extrapolating models developed for condensation inside macroscale plain tubes. Among the models which have been used for comparison with the present data, the one that provides the most accurate prediction is the correlation by Cavallini et al. [29], which was developed from a database referred to macroscale tubes. These results suggest that the same correlations used for condensation in conventional tubes can be used in the design of minichannel condensers, provided that the mass velocity is high enough and that the channel presents a circular cross-section. Further investigation has to be carried out before extending similar conclusions to non-circular minichannels.

Acknowledgments

The authors would like to acknowledge the support of EC through the project HPRN-CT-2002–2004, of MIUR through PRIN project and of ESA through ENCOM project.

References

[1] S.G. Kandlikar, W.J. Grande, Evolution of microchannel flow passages – thermohydraulic performance and fabrication technology, Heat Transfer Eng. 24 (1) (2003) 3–17.
[2] A. Cavallini, G. Censi, D. Del Col, L. Doretti, G.A. Longo, L. Rossetto, Condensation of Halogenated Refrigerants inside Smooth Tubes, HVAC&R Research 8 (4) (2002) 429–451.
[3] A. Cavallini, L. Doretti, M. Matkovic, L. Rossetto, Update on condensation heat transfer and pressure drop in minichannels, Heat Transfer Eng. 27 (4) (2006) 74–87.
[4] S. Garimella, Condensation in minichannels and microchannels, in: S.G. Kandlikar, S. Garimella, D. Li, S. Colin, M.R. King (Eds.), Heat Transfer and Fluid Flow in Minichannels and Microchannels, Elsevier Ltd., 2006.
[5] C.-Y. Yang, R.L. Webb, Condensation of R-12 in small hydraulic diameter extruded aluminum tubes with and without micro-fins, Int. J. Heat Mass Transfer 39 (1996) 791–800.
[6] M. Zhang, R.L. Webb, Correlation of two-phase friction for refrigerants in small-diameter tubes, Exp. Therm. Fluid Sci. 25 (2001) 131–139.
[7] R.L. Webb, K. Ermis, Effect of hydraulic diameter on condensation of R-134a in flat, extruded aluminum tubes, Enhanced Heat Transfer 8 (2001) 77–90.
[8] Y.-Y. Yan, T.-F. Lin, Condensation heat transfer and pressure drop of refrigerant R134a in a small pipe, Int. J. Heat Mass Transfer 42 (1999) 697–708.
[9] A. Vardhan, E.E. Dunn, Heat Transfer and Pressure Drop Characteristics of R-22, R-134a and R-407C in Microchannel Tubes, ACRC TR-133, University of Illinois at Urbana-Champaign, 1997.
[10] W. Wang Wei-Wen, T.D. Radcliff, R.N. Christensen, A condensation heat transfer correlation for millimetre-scale tubing with flow regime transition, Exp. Therm. Fluid Sci. 26 (2002) 473–485.
[11] S. Garimella, Condensation flow mechanisms in microchannels: basis for pressure drop and heat transfer models, Heat Transfer Eng. 25/3 (2004) 104–116.
[12] N.-H. Kim, J.-P. Cho, J.-O. Kim, B. Youn, Condensation heat transfer of R-22 and R-410A in flat aluminum multi-channel tubes with or without micro-fins, Int. J. Refrig. 26 (2003) 830–839.
[13] M.H. Kim, J.S. Shin, C. Huh, T.J. Kim, K.W. Seo, A study of condensation heat transfer in a single mini-tube and review of Korean micro- and mini-channel studies, in: First International Conference on Microchannels and Minichannels, Rochester, NY, 2003, pp. 47–58.
[14] S. Koyama, K. Kuwara, K. Nakashita, Condensation of refrigerant in a multi-port channel, in: First International Conference on Microchannels and Minichannels, Rochester, NY, 2003, pp. 193–205.
[15] J.R. Baird, D.F. Fletcher, B.S. Haynes, Local condensation heat transfer rates in fine passages, Int. J. Heat Mass Transfer 46 (2003) 4453–4466.
[16] A. Cavallini, D. Del Col, L. Doretti, M. Matkovic, L. Rossetto, C. Zilio, Condensation heat transfer and pressure gradient inside multiport minichannels, Heat Transfer Eng. 26 (3) (2005) 45–55.
[17] T.M. Bandhauer, A. Agarwal, S. Garimella, Measurement and modeling of condensation heat transfer coefficients in circular microchannels, in: Proceedings of ICMM2005, The 3rd International Conference on Microchannels and Minichannels, Toronto, ON, Canada, 2005, ICMM2005-75248.
[18] T. Baummer, E. Cetegan, M. Ohadi, S. Dessiatoun, Force-fed evaporation and condensation utilizing advanced micro-structured surfaces and micro-channels, Microelectron. J. 39 (7) (2008) 975–980.
[19] L. Friedel, Improved friction pressure drop correlations for horizontal and vertical two phase pipe flow, in: European Two Phase Flow Group Meeting, Ispra, Italy, 1979, Paper E2.
[20] Z. Rouhani, E. Axelsson, Calculation of void volume fraction in the subcooled and quality boiling regions, Int. J. Heat Mass Transfer 13 (1970) 383–393.
[21] A. Cavallini, D. Del Col, M. Matkovic, L. Rossetto, Frictional pressure drops during vapour-liquid flow in minichannels: experimental data and modelling, in: Micro/Nanoscale Heat Transfer International Conference, Tainan, Taiwan, 2008, MNHT2008-52282.
[22] VDI heat atlas/ed. Verein Deutscher Ingenieure, VDI-Gesellschaft Verfahrenstechnik und Chemieingenieurwesen (GVC) [Transl. J. W. Fullarton]. – Düsseldorf, VDI-Verl., 1993.
[23] VDI-Wärmeatlas, Verein Deutscher Ingenieure, VDI-Gesellschaft Verfahrenstechnik und Chemieingenieurwesen (GVC), Springer-Verlag, Berlin, Hedelberg, New York, 2002.
[24] A. Cavallini, G. Censi, D. Del Col, L. Doretti, G.A. Longo, L. Rossetto, Experimental investigation on condensation heat transfer and pressure drop of new HFC refrigerants (R134a, R125, R32, R410A, R236ea) in a horizontal tube, Int. J. Refrig. 24 (2001) 73–87.
[25] H.M. Soliman, Mist-annular transition during condensation and its influence on the heat transfer mechanism, Int. J. Multiphase Flow 12 (2) (1986) 277–288.
[26] J.W. Coleman, S. Garimella, Two-phase flow regime transitions in microchannel tubes: the effect of hydraulic diameter, ASME HTD 366-4 (2000) 71–83.
[27] K.W. Moser, R.L. Webb, B. Na, A new equivalent Reynolds number model for condensation in smooth tubes, J. Heat Transfer 120 (1998) 410–417.
[28] P.G. Kosky, F.W. Staub, Local condensing heat transfer coefficients in the annular flow regime, AIChE J. 17 (1971) 1037–1043.
[29] A. Cavallini, G. Censi, D. Del Col, L. Doretti, M. Matkovic, L. Rossetto, C. Zilio, Condensation in horizontal smooth tubes, a new heat transfer model for heat exchanger design, Heat Transfer Eng. 27 (8) (2006) 31–38.